Laboratory Investigation (2020) 100:1436–1446
https://doi.org/10.1038/s41374-020-0447-y

ARTICLE

MiR-185-5p ameliorates endoplasmic reticulum stress and renal fibrosis by downregulation of ATF6

Quan Yuan[1] · Tianhua Xu[2] · Ying Chen[2] · Wei Qu[2] · Dan Sun[2] · Xiaodan Liu[2] · Li Sun[2]

Received: 18 October 2019 / Revised: 22 May 2020 / Accepted: 24 May 2020 / Published online: 8 June 2020

Abstract

Endoplasmic reticulum (ER) stress is considered an important factor in the formation of fibrosis. Therefore, modulation of ER stress may represent a promising therapeutic strategy in renal fibrosis. MiR-185-5p has been identified to be implicated in TGF-β1-induced renal fibrosis; however, it is largely unknown whether and how miR-185-5p regulates ER stress in renal fibrosis. In this study, we demonstrated that miR-185-5p directly bound to ATF6, an ER stress-related protein, and downregulated the expression thereof. We subsequently constructed an in vitro model of renal fibrosis using HK2 cells treated with TGF-β1, and found that miR-185-5p attenuated ER stress and dedifferentiation of tubular epithelia by suppression of ATF6. In addition, we constructed an in vivo mouse model using unilateral urethral obstruction (UUO). Our in vivo findings showed that miR-185-5p reduced the expression of ER stress-related proteins and inhibited epithelial dedifferentiation via downregulation of ATF6, thereby improving UUO-induced renal fibrosis. Overall, our findings revealed that miR-185-5p exerts beneficial effects in renal fibrosis. Thus, the miR-185-5p/ATF6 regulatory pathway may be a potential target for therapeutic intervention in renal fibrosis.

Introduction

Renal fibrosis, characterized by fibroblast proliferation and extracellular matrix (ECM) accumulation, is an important pathological characteristic in chronic kidney disease (CKD) induced by various causes. Renal fibrosis is an aberrant wound-healing response to chronic injury. After the initial epithelial injury, kidney-resident cells are activated, leading to ongoing inflammation, and in turn promote the activation of fibroblasts and tubular epithelial cells, or the transition into ECM-secreting myofibroblasts. Finally, continuous deposition of ECM leads to trauma of renal parenchyma, loss of renal function, and end-stage renal failure [1, 2]. Clinically, effective treatment for renal fibrosis only involves dialysis or kidney transplantation. Therefore, exploring novel therapeutic targets for antifibrotic therapy is of utmost importance. Unilateral ureteral obstruction (UUO) induced in rodents is a well-established model of renal fibrosis involving urinary pathway obstruction. Continuous urinary retention results in elevated renal pressure, reduced renal blood flow, and a reduced glomerular filtration rate, thereby exacerbating injury of the renal parenchyma, which ultimately leads to irreversible renal fibrosis [3, 4]. As characterized by rapid tubular atrophy and interstitial fibrosis and matrix deposition, UUO is widely used to study tubulointerstitial fibrosis [5].

Endoplasmic reticulum (ER) stress is a cytoprotective mechanism to cope with environmental stimuli, such as reactive oxygen species, glucose deprivation, and aberrant regulation of calcium. To maintain homeostasis of the ER, ER stress initiates three branches of unfolded protein response (UPR): (1) The PERK/eIF2α/ATF4 branch. During ER stress, PERK becomes activated via dimerization and autophosphorylation, resulting in phosphorylation of eIF2α and inhibition of protein translation, and phosphorylated eIF2α facilitates the expression of transcription factor ATF4 [6, 7]. (2) The IRE1/XBP1 branch. In response to ER stress, IRE1 unbinds from GRP78 (also known as

Supplementary information The online version of this article (https://doi.org/10.1038/s41374-020-0447-y) contains supplementary material, which is available to authorized users.

✉ Li Sun
sunlicmu1974@163.com

[1] Department of Orthopedics, Shengjing Hospital of China Medical University, Shenyang 110004, People's Republic of China

[2] Department of Nephrology, The First Hospital of China Medical University, Shenyang 110001, People's Republic of China

BiP), becomes activated, and leads to further splicing of XBP1. The newly produced spliced XBP1 (sXBP1) serves as a transcription factor to regulate the expression of ER proteins [8, 9]. (3) The ATF6 branch. When ER stress occurs, ATF6 dissociates from GRP78, and transports from the ER membrane to the Golgi apparatus. After cleaving by serine proteases, the active form of ATF6 translocates to the nucleus and induces the expression of ER stress-responsive genes [10, 11]. However, overwhelming or prolonged ER stress results in the activation of proapoptotic pathways, epithelial cell dedifferentiation toward a mesenchymal phenotype, and inflammatory responses, which play an important role in the formation of fibrosis [12, 13]. ER stress is involved in the pathological process of renal diseases [14], and is closely related to the onset of renal fibrosis [15]. In the UUO model of renal fibrosis, ER stress has been demonstrated [16], and targeted inhibition of ER stress may inhibit renal fibrosis [17, 18].

ATF6 (activating transcription factor 6) is a major sensor that becomes activated when ER stress induces UPR. Active ATF6 translocates to the nucleus to regulate ER proteins at the transcriptional level, including GRP78, C/EBP homologous protein (CHOP), XBP1, protein disulfide isomerase, and calreticulin [10, 19–21]. Prior studies have noted the important role of ATF6 in organ fibrosis. Surveys conducted by Baek et al. have shown that selected ER stress pathways lead to increased expression of TGF-β-induced ATF6 in human and murine pulmonary fibroblasts [22]. In renal fibrosis, the ATF6–CHOP proapoptotic pathway has been reported to be activated by prolonged ER stress [23].

MicroRNA (miRNA) is a type of small noncoding RNA, which regulates the expression of target genes at the post-transcriptional level by degrading mRNA [24]. It has been confirmed that miRNA can be a regulator of tissue fibrosis under pathological conditions in CKD, and exerts as potential therapeutic targets [25, 26]. For example, the intrarenal expression of miR-200a, miR-200b, and miR-429 is increased in patients with hypertensive nephrosclerosis [27, 28]. In the past few years, most studies involving miR-185-5p were focused on its involvement in tumor progression [29, 30]. In a recent study, it was demonstrated that miR-185-5p inhibited dedifferentiation and proliferation in TGF-β1-induced renal fibrosis [31], thereby suggesting that it may play a role in renal pathology. In addition, miR-185-5p has also been proven to suppress ER stress-induced apoptosis in the heart [32]. However, whether miR-185-5p affects renal fibrosis by regulating ER stress remains to be elucidated.

In this study, we aimed to identify the role and regulation of miR-185-5p in renal fibrosis. We found that ER stress-related protein ATF6 is a target gene of miR-185-5p based on the microRNA target prediction databases (StarBase and TargetScan), and we first demonstrated that miR-185-5p downregulated the expression of ATF6 by directly binding to recognition sites within the 3′-UTR. In addition, we induced renal fibrosis in TGF-β1-exposed HK2 cells and in a mouse model via UUO, and demonstrated that miR-185-5p-mediated downregulation of ATF6 resulted in alleviation of ER stress and ER stress-induced dedifferentiation. Taken together, our findings provided a novel mechanistic explanation for ER stress and renal fibrosis, through the miR-185-5p/ATF6 regulatory pathway.

Materials and methods

Cell culture

HK2 cells (human renal proximal tubular epithelial cell line) were cultured in MEM (Procell Life Science & Technology, China) supplemented with 10% fetal bovine serum (FBS, Biological Industries, Israel). In addition, 293 T cells were cultured in DMEM (Procell Life Science & Technology, China) supplemented with 10% FBS. Cells were grown in a humidified environment at 37 °C and 5% CO_2.

Cell transfection and treatment

Hsa-miR-185-5p mimics and the negative control (NC) or ATF6 overexpression plasmids and vector plasmids (Invitrogen) were co-transfected into HK2 cells accordingly. Transfections were performed using Lipofectamine 2000 (Invitrogen, 11668-019) with Opti-MEM medium following the manufacturer's guidelines. After culturing for 48 h, cells were harvested, and the transfection efficiency was determined. Subsequently, cells were incubated with 5 ng/mL TGF-β1 for 24 h. Groups were as follows: 1: control, 2: TGF-β1, 3: TGF-β1 + NC, 4: TGF-β1 + hsa-miR-185-5p mimics, 5: TGF-β1 + hsa-miR-185-5p mimics + vector, and 6: TGF-β1 + hsa-miR-185-5p mimics + ATF6 OE.

Real-time PCR

Total RNA was extracted using the RNAsimple Total RNA Kit (Tiangen Biotech, DP419) following the manufacturer's guidelines. RNA was reverse-transcribed by M-MLV (Tiangen Biotech, NG212). Real-time PCR was carried out using 2× Taq PCR MasterMix (Tiangen Biotech, KT201) and SYBR Green (Solarbio, SY1020). Primers used were as follows: homo ATF6: forward: 5′-ATAA GCCTGTCACTGGTC-3′, reverse: 5′-TTTGTTTGAGTCT TGGGT-3′, mus ATF6: forward: 5′-CTGGACGAGGTGG TGTCA-3′, reverse: 5′-CTCTTCGGGATTCTTGCT-3′, homo GAPDH: forward: 5′-GACCTGACCTGCCGTCT AG-3′, reverse: 5′-AGGAGTGGGTGTCGCTGT-3′, mus

GAPDH: forward: 5′-TGTTCCTACCCCCAATGTGTCC GTC-3′, reverse: 5′-CTGGTCCTCAGTG TAGCCCAAGA TG-3′, mmu/hsa-miR-185-5p: RT primer: 5′-GTTGGCTCT GGTGCAGGGTCCGAGGTATTCGCACCAGAGCCAA CTCAGGA-3′, forward: 5′-TGGAGAGAAAGGCAGTT CCTGA-3′, reverse: 5′-GTGCAGGGTCCGAGGTATT C-3′, hsa-U6: RT primer: 5′-GTTG GCTCTGGTG CAGGGTCCGAGGTATTCGCACCAGAGCCAACAAA ATATGG-3′, forward: 5′-GCTTCGGCAGCACATATA CT-3′, reverse: 5′-GGTGCAGGGTCCGAGGTAT-3′, and mmu-U6: RT primer: 5′-GTTGGCTCTGGTGCAGGGT CCGAGGTA TTCGCACCAGAGCCAACAAAAATATG G-3′, forward: 5′-CGCAAGGATGACAC GCAAAT-3′, reverse: 5′-GGTGCAGGGTCCGAGGTAT-3′. GAPDH and U6 served as internal controls for mRNA and miRNA, respectively, and the fold change relative to the control was calculated by the $2^{-\Delta\Delta Ct}$ method.

Nuclear protein extraction

A nuclear protein extraction kit (Solarbio, R0050) containing cytoplasmic lysis buffer and nuclei lysis buffer was used to extract cytoplasmic and nuclear protein from cells or tissue.

In brief, cells were lysed in 200 μL of cytoplasmic lysis buffer on ice for 10 min. The mixture was vortexed for 10 s, then centrifuged at 12,000 × *g* for 10 min at 4 °C. The supernatant contained cytoplasmic proteins. The pellet was resuspended in 50 μL of nuclei lysis buffer and kept on ice for 10 min. Nuclear proteins were extracted by centrifugation at 12,000 × *g* for 10 min at 4 °C. The supernatant contained the nuclear extract.

Renal tissue was first cut into small pieces and mechanically homogenized on ice with PBS. After centrifugation at 500 × *g* for 3 min at 4 °C, the pellet was lysed in 200 μL of cytoplasmic lysis buffer. Subsequent processing steps were similar as the steps mentioned above for the extraction of nuclear protein from cells.

Western blot analysis

Cells or tissues were lysed with RIPA lysis buffer (Solarbio, R0010) added with phenylmethylsulfonyl fluoride. The protein concentration was determined by a BCA Protein Assay Kit (Solarbio, PC0020). Protein lysates were separated by 8–15% SDS-PAGE and electrophoretically transferred onto PVDF membranes. Membranes were incubated overnight with primary antibodies at 4 °C followed by horseradish peroxidase-conjugated goat anti-rabbit or goat antimouse IgG (Solarbio) at 37 °C for 45 min. The immunoreactivity was visualized by ECL reagent (Solarbio, PE0010). The gray values were analyzed with Gel-pro Analyzer Software (Media Cybernetics, Bethesda, MD, USA). Antibodies used were as follows: ATF6 antibody (Proteintech, 24169-1-AP), sXBP1 antibody (CST, #12782), IRE1α antibody (Affinity, DF7709), p-IRE1α (Ser724) antibody (Affinity, AF7150), PERK antibody (Affinity, AF5304), p-PERK (Thr981) antibody (Thermo Fisher, PA5-40294), ATF4 antibody (Proteintech, 10835-1-AP), eIF2α antibody (Affinity, AF6087), p-eIF2α (Ser51) antibody (Affinity, AF3087), CHOP antibody (Affinity, DF6025), GRP78 antibody (Affinity, AF5366), cleaved-caspase 12 antibody (Abcam, ab140882/GeneTex, GTX59923), fibronectin antibody (Proteintech, 15613-1-AP), collagen I antibody (Affinity, AF0134), collagen III antibody (Affinity, AF5457), E-cadherin antibody (Affinity, AF0131), α-SMA antibody (Affinity, AF1032), TGF-β1 antibody (Affinity, AF1027), GAPDH antibody (Proteintech, 60004-1-Ig), and Histone H3 antibody (GeneTex, GTX122148).

Double-immunofluorescence staining

For cells grown on chamber slides, slides were fixed for 15 min with 4% paraformaldehyde and permeabilized with 0.1% Triton X-100 for 30 min. For tissue sections, sections were heated at 60 °C for 2 h, followed by paraffin removal and rehydration. Antigen retrieval was performed at a subboiling temperature for 10 min. Subsequently, both cell slides and tissue sections were blocked with goat serum. Primary antibodies directed against E-cadherin (Ms) and α-SMA (Rb) were diluted in PBS (1:200). The antibody combination of E-cadherin-α-SMA was added to each section, respectively, and incubated overnight at 4 °C. Then, sections were washed, and incubated with FITC- or Cy3-conjugated secondary goat antimouse or rabbit antibody (1:200) for 90 min. Nuclei were stained with DAPI (Beyotime, China). After three additional washes with PBS for 5 minutes, sections were sealed by anti-fade reagent. Cells were examined at 400× magnification using a microscope.

Dual-luciferase reporter assay

To investigate whether ATF6 expression was regulated by miR-185-5p, a dual-luciferase reporter assay was employed. In brief, 2×10^5 293 T cells (Procell Life Science & Technology, China) were transfected using Lipofectamine 2000 (Invitrogen) with 0.5 μg of pmirGLO vetor (Promega, E133A) containing wild type (wt) or mutant (mut) ATF6 3′ UTR, along with 25 pmol hsa-miR-185-5p or mmu-miR-185-5p mimics, and their NC. Firefly and Renilla luciferase activity were determined by a dual-luciferase reporter assay system (Promega, E1910) using a multimode microplate plate reader (Infinite M200PRO, TECAN, Switzerland).

Animals and grouping

Male C57BL/6 mice (20–22 g) were obtained from Changsheng Biotechnology (Liaoning, China). Mice were housed in an experimental animal facility, at a constant temperature (22 ± 1 °C) and humidity (45–55%), under a consistent light cycle (12-h light/dark). Food and water were allowed ad libitum. Mice were randomly divided into four groups ($n = 12$ per group): (1) sham, (2) UUO, (3) UUO + LV NC, and (4) UUO + LV-mmu-miR-185-5p. All surgical and experimental procedures were performed in accordance with the Guide for Laboratory Animal Care and Use, and approved by the Institutional Animal Ethics Committee of China Medical University.

Induction of unilateral ureteral obstruction

Mice were anesthetized using pentobarbital (50 mg/kg, intraperitoneally), after which the left ureter was isolated and exposed through an abdominal incision. A 3-mm steel wire segment was placed adjacent to the left ureter, and a nylon thread was tied around the ureter and the steel wire at the ureteropelvic junction. The wire was removed, leaving the ligation around the ureter. Subsequently, the incision was closed. Sham-operated (Sham) mice were subjected to an identical procedure without ligation of the left ureter.

Lentivirus transfection

After the induction of UUO, mice received a tail-vein injection. For mice in the UUO + LV NC and UUO + LV-mmu-miR-185-5p groups, 0.2 mL of lentivirus plasmid (1×10^9 TU/mL) containing the NC or mmu-miR-185-5p was injected through the tail vein. On the 15th day after setting up the model, mice were euthanized and kidneys were collected.

Histological examination

Renal tissues from mice were fixed, embedded in paraffin, and cut into 5-μm-thick sections. After dewaxing and rehydrating, sections were stained with periodic acid Schiff (PAS) reagent (Anhui Leagene Biotechnology, China) or Masson's trichrome solution (Sinopharm Chemical Reagent, China). Sections were visualized using an optic microscopy (DP73, Olympus, Japan) at 200× magnification. Semiquantification of PAS staining was performed to evaluate tubular injury. Tubular injury was defined as tubular atrophy with interstitial fibrosis, tubular dilation, tubular cast formation, thickening of the tubular basement membrane, and sloughing of tubular epithelial cells, and scores between 0 and 5 were given [33] as follows: 0: no tubular injury, 1: <10% of tubules injured, 2: 10–25% of tubules injured, 3: 26–50% of tubules injured, 4: 51–75% of tubules injured, and 5: >75% of tubules injured. The positive area of Masson's trichrome staining (blue) was calculated using Image-Pro Plus software.

Statistical analysis

Data are expressed as the mean ± standard deviation (SD). Data were analyzed using one-way analysis of variance (ANOVA) followed by Tukey's test. $P < 0.05$ was considered statistically significant.

Results

MiR-185-5p bound to ATF6 and downregulated the expression thereof

The expression levels of miR-185-5p and ATF6 were determined after in vitro transfection. The results showed that miR-185-5p was prominently upregulated, and ATF6 was downregulated in HK2 cells after transfection with hsa-miR-185-5p mimics. In addition, overexpression of ATF6 effectively elevated its expression (Fig. 1a–c), which validated that the transfection was successful. A bioinformatic target prediction using StarBase and TargetScan showed that the putative binding site for miR-185-5p was present in the 3′UTR of ATF6. Wild-type and mutated sequences of ATF6 3′UTR, as well as the matched sequence for miR-185-5p, were shown in Fig. 1d. The results of the luciferase activity analysis demonstrated the direct binding of miR-185-5p to ATF6 (Fig. 1e). Taken together, these findings indicated that ATF6 was a direct target of miR-185-5p, and that miR-185-5p negatively regulated the expression of ATF6.

MiR-185-5p alleviated the degree of ER stress by regulating ATF6 in TGF-β1-induced HK2 cells

TGF-β1 has been identified as a master regulator that drives fibrosis in variety of disease models [34]. In the current study, we established an in vitro model by inducing HK2 cells with TGF-β1. To investigate whether the miR-185-5p level was altered during renal fibrosis, real-time PCR was performed. The results illustrated that TGF-β1-treated HK2 cells showed significantly decreased level of miR-185-5p, and transfection of miR-185-5p mimics restored this reduction (Fig. 2a). As shown in Fig. 2b–e, the total protein level of ATF6 was enhanced in HK2 cells exposed to TGF-β1, resulting in an increase in ATF6 translocation into the nucleus. Consequently, the expression of ER stress-responsive genes, including GRP78 and CHOP, initiated by nuclear ATF6 was increased. However, pretreatment

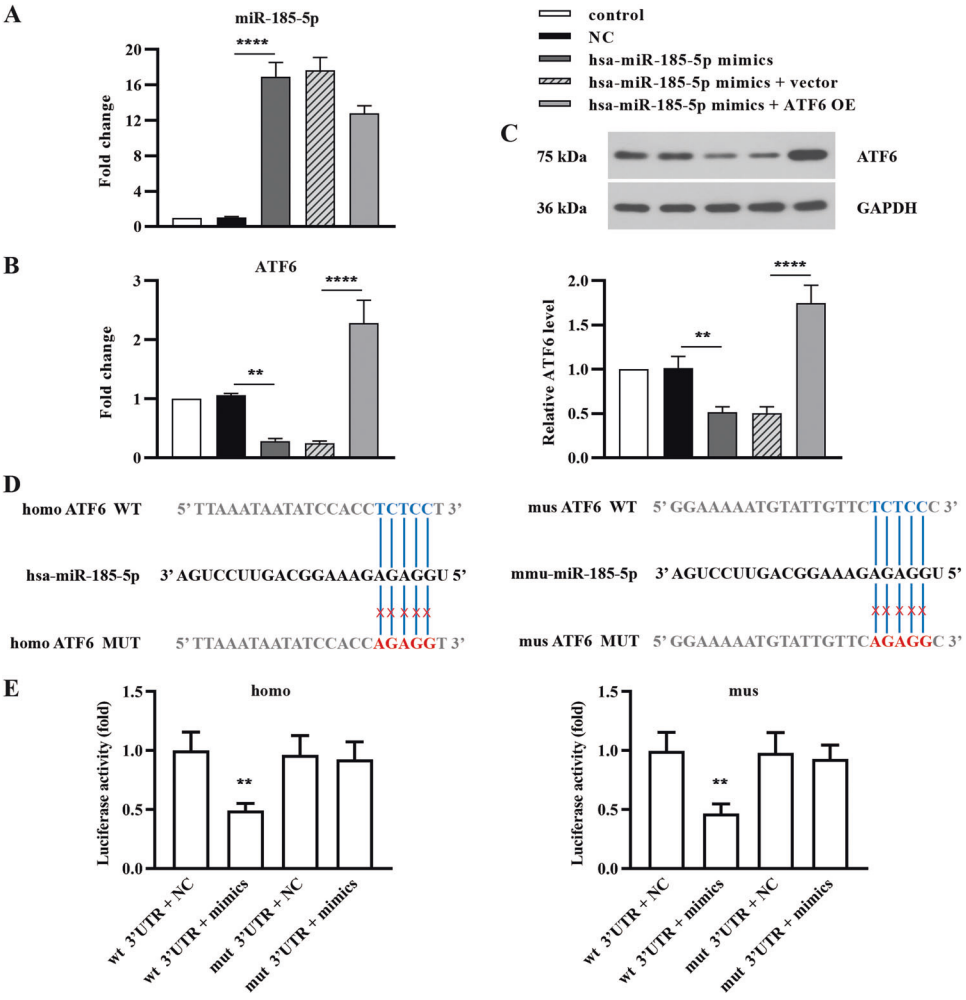

Fig. 1 MiR-185-5p binds to ATF6 and downregulates the expression thereof. a Real-time PCR analysis of miR-185-5p in HK2 cells. **b** ATF6 mRNA level as determined by real-time PCR. **c** ATF6 protein expression and quantitative analysis in HK2 cells. **d** Sequence alignment of the predicted miR-185-5p-binding site in the 3′UTR of ATF6 for species, including *Homo sapiens* (hsa) and *Mus musculus* (mmu). **e** Binding of miR-185-5p and ATF6 measured by the dual-luciferase reporter assay. Data are presented as the mean ± SD ($n = 3$) by one-way ANOVA with Tukey's test for multiple comparisons (**$P < 0.01$; ****$P < 0.0001$).

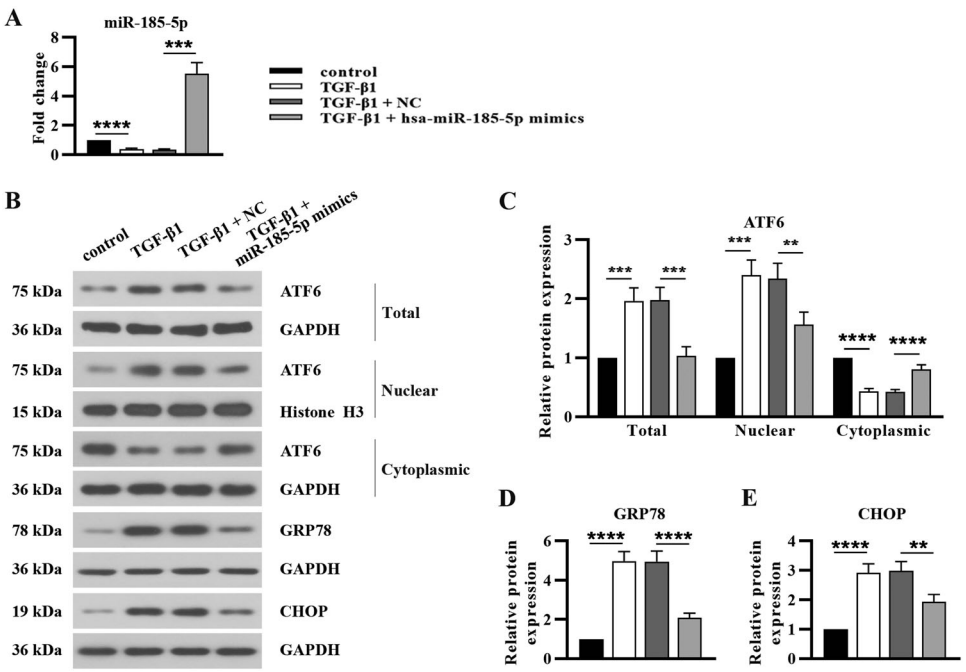

Fig. 2 MiR-185-5p alleviates the degree of endoplasmic reticulum stress in TGF-β1-induced HK2 cells. a Real-time PCR analysis of miR-185-5p in TGF-β1-induced HK2 cells. **b** Western blot analysis of ATF6, GRP78, and CHOP proteins in HK2 cells that were transfected with miR-185-5p mimics or scrambled RNA (NC) after TGF-β1 treatment. **c–e** Quantitative analysis of the relative protein level in (**b**). Data are presented as the mean ± SD ($n = 3$) with the statistical significance calculated from one-way ANOVA with Tukey's test (**$P < 0.01$; ***$P < 0.001$; ****$P < 0.000$).

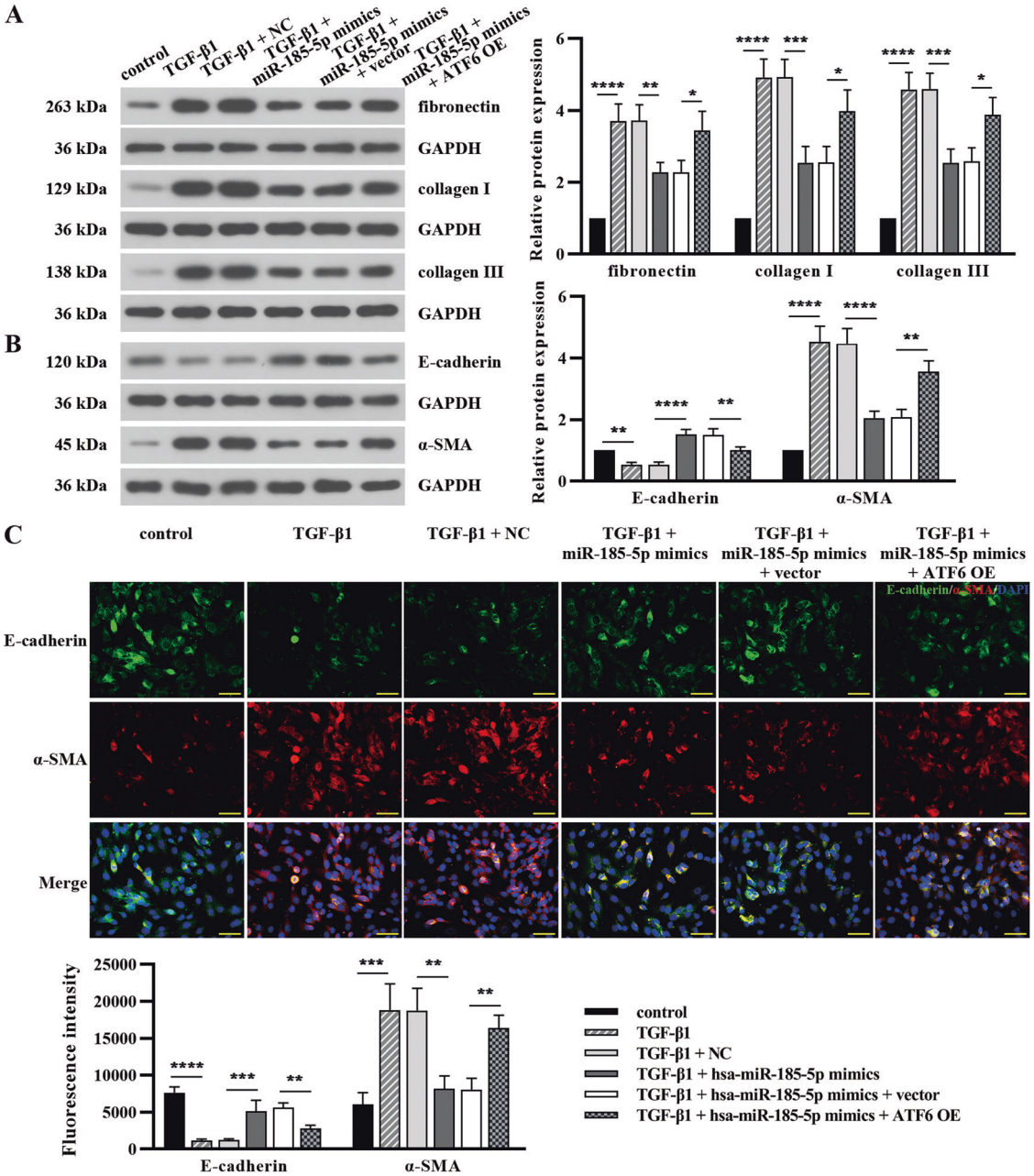

Fig. 3 MiR-185-5p prevents extracellular matrix accumulation and dedifferentiation of TGF-β1-induced HK2 cells by downregulating ATF6. a Expression of fibronectin, collagen I, and collagen III, and quantitative analysis of relative protein expression. **b** Western blot and quantitative analysis were employed to determine dedifferentiation-associated markers in HK2 cells. **c** Immunofluorescence staining of E-cadherin (green) and α-SMA (red), and quantitative analysis of the staining intensity. Scale bar, 50 μm. Statistically significant differences are presented as the mean ± SD ($n = 3$) by one-way ANOVA with Tukey's test for multiple comparisons.

with miR-185-5p mimics reduced the total protein level of ATF6 in TGF-β1-induced HK2 cells, and further caused the decreased level of nuclear ATF6 and relatively increased cytoplasmic ATF6. ATF6 induced GRP78, and CHOP expression was blocked by overexpression of miR-185-5p. We further performed Western blot analysis on ATF6-silenced HK2 cells (Supplementary Fig. 1). The results showed that ATF6 knockdown resulted in decreased levels of GRP78 and CHOP, which confirmed that miR-185-5p regulated ATF6, thereby affecting the expression of GRP78 and CHOP. Moreover, miR-185-5p suppressed activation of the IRE1/XBP1 branch (Supplementary Fig. 2A, B) and the PERK/eIF2α/ATF4 branch (Supplementary Fig. 2C, D) in TGF-β1-induced HK2 cells. Combined, these results revealed that miR-185-5p mitigated the degree of ER stress by downregulating ATF6 in TGF-β1-exposed HK2 cells.

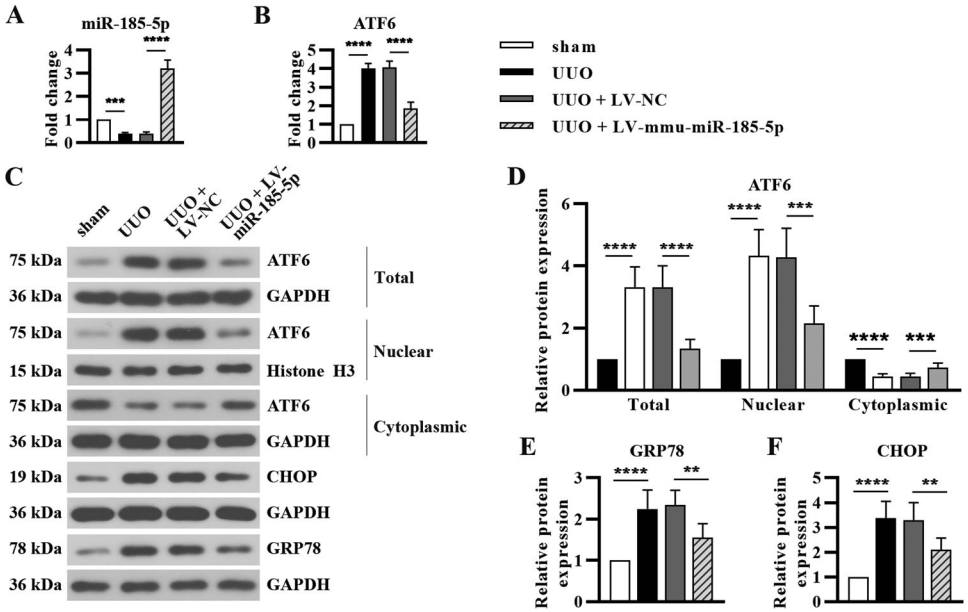

Fig. 4 MiR-185-5p alleviates the degree of endoplasmic reticulum stress in a mouse model of unilateral urethral obstruction. a Real-time PCR of miR-185-5p in the kidney of unilateral urethral obstruction (UUO) mice ($n = 6$ per group). **b** ATF6 mRNA level in the kidney of UUO mice. **c** Western blot analysis of ATF6, GRP78, and CHOP proteins in the kidney of UUO mice. **d–f** Quantification of the gray values of Western blots in (**c**). Data are presented as the mean ± SD ($n = 6$) based on one-way ANOVA with Tukey's test of three independent experiments. $^{**}P < 0.01$; $^{***}P < 0.001$; $^{****}P < 0.0001$.

MiR-185-5p prevented ECM accumulation and dedifferentiation of TGF-β1-induced HK2 cells by downregulating ATF6

To investigate the role of miR-185-5p in ECM accumulation, we determined the expression of ECM components, including fibronectin, collagen I, and collagen III. In TGF-β1-induced HK2 cells, the expression of fibronectin, collagen I, and collagen III was markedly higher when compared with that of control cells. Administration of hsa-miR-185-5p mimics blocked the expression of these proteins. However, this effect was reversed by overexpression of ATF6 (Fig. 3a). Considering that ER stress induces dedifferentiation, we determined the levels of E-cadherin (epithelial marker) and α-SMA (mesenchymal marker) by Western blot analysis and immunofluorescence. As shown in Fig. 3b, c, TGF-β1-induced dedifferentiation of HK2 cells, as evidenced by reduced E-cadherin and increased expression of α-SMA. In contrast, miR-185-5p increased the expression of E-cadherin and restrained α-SMA expression. However, these changes in protein expression were reversed by ATF6 overexpression. Thus, these findings indicated that miR-185-5p attenuated ECM accumulation and dedifferentiation through downregulating ATF6 in TGF-β1-induced HK2 cells.

MiR-185-5p alleviated the degree of ER stress in a mouse model of UUO

Next, we tested whether miR-185-5p had a mitigative effect on ER stress in vivo using a mouse model of UUO. First, we performed real-time PCR to determine the levels of miR-185-5p and ATF6 in the kidneys of UUO mice. In the UUO group, miR-185-5p was downregulated, and ATF6 was upregulated. However, the level of ATF6 was decreased when mice were injected with miR-185-5p lentivirus (Fig. 4a, b). As shown by Western blot analysis, miR-185-5p inhibited the UUO-induced increase in total ATF6 protein level, as well as the subsequent ATF6 nuclear translocation, and increased the expression of CHOP and GRP78 (Fig. 4c–f). Furthermore, we found that miR-185-5p suppressed the activation of the IRE1/XBP1 and PERK/eIF2α/ATF4 branches in the UUO model (Supplementary Fig. 3). Taken together, these findings verified that miR-185-5p alleviated the degree of ER stress in the UUO model.

MiR-185-5p prevented renal fibrosis and epithelial dedifferentiation in a mouse model of UUO

To confirm the role of miR-185-5p in renal fibrosis and epithelial dedifferentiation in the UUO model, we first examined the degree of fibrosis by Masson staining. As shown in Fig. 5a, the area of interstitial fibrosis was increased in the UUO group, while administration of miR-185-5p lentivirus decreased the fibrotic area. The expression of profibrotic proteins as determined by Western blot analysis was consistent with those of the Masson staining (Fig. 5b). Next, the effect of miR-185-5p on epithelial dedifferentiation was further evaluated. UUO surgery resulted in dedifferentiation of tubular epithelia, as evidenced by blocked expression and reduced fluorescence intensity of E-cadherin, as well as by upregulated expression and enhanced fluorescence intensity of α-SMA (Fig. 5c, d). We found that this phenomenon could be improved in the UUO + LV-mmu-miR-185-5p group.

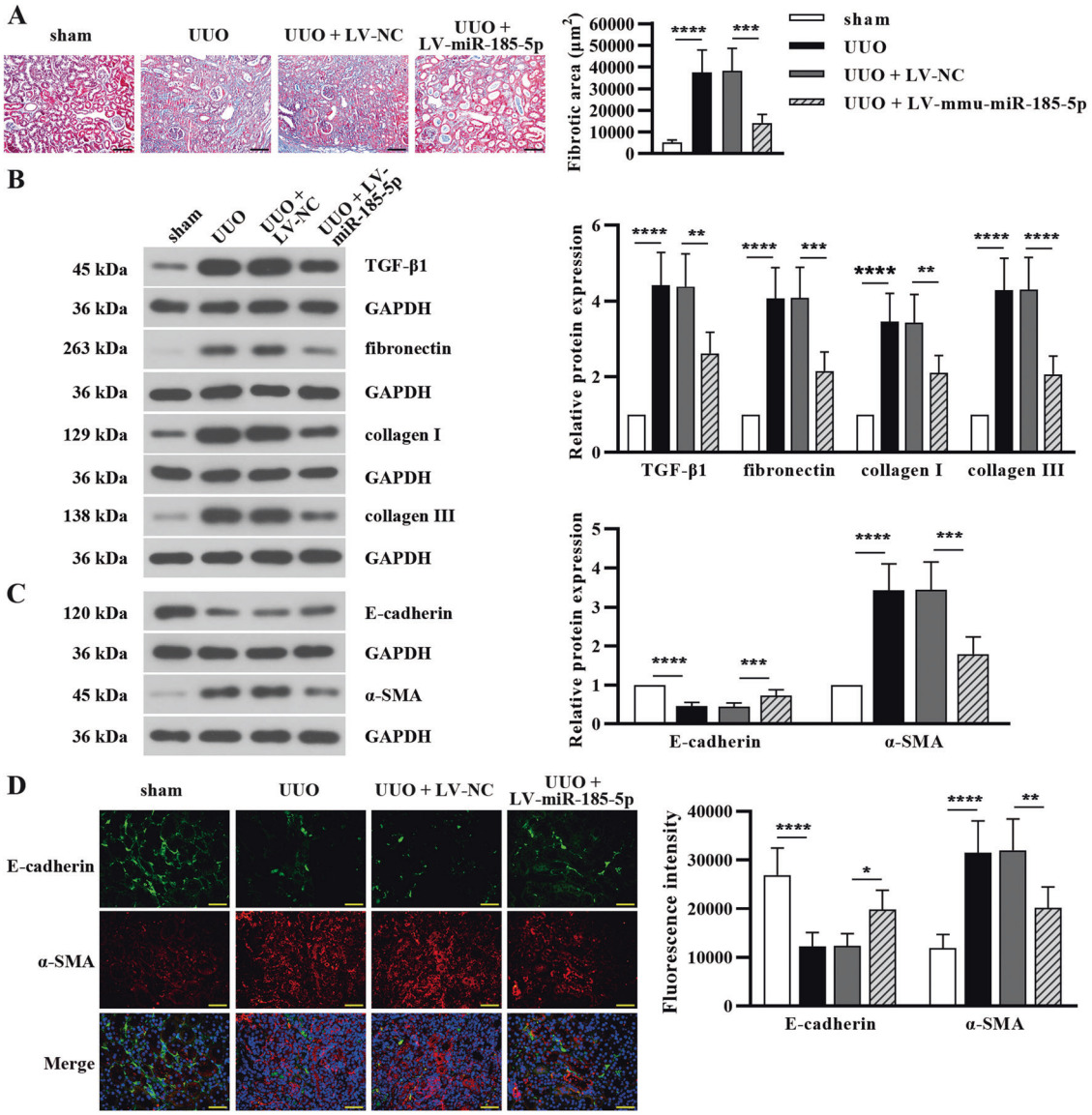

Fig. 5 MiR-185-5p prevents renal fibrosis and epithelial dedifferentiation in a mouse model of unilateral urethral obstruction. **a** Masson staining and quantitative analysis of representative tissue sections from each group ($n = 6$). Scale bar, 100 μm. **b** The expression of profibrotic proteins TGF-β1, fibronectin, collagen I, and collagen III in the kidney of unilateral urethral obstruction (UUO) mice, and quantitative analysis. **c** Western blot analysis of E-cadherin and α-SMA, and quantitative analysis of relative protein expression. **d** Immunofluorescence staining of E-cadherin (green) and α-SMA (red), and quantitative analysis of the staining intensity. Scale bar, 50 μm. Statistical analyses were based on one-way ANOVA with Tukey's test for multiple comparisons.

Thus, these data suggested that miR-185-5p protected against renal fibrosis and epithelial dedifferentiation.

Effects of miR-185-5p on renal structure in a mouse model of UUO

We evaluated renal injury using PAS staining, and semi-quantitative analysis was employed. Significant tubular damage was observed in the kidney of UUO mice, as evidenced by tubular atrophy and interstitial fibrosis. However, this damage was attenuated after the injection of miR-185-5p lentivirus (Fig. 6a, b). These data implied that miR-185-5p improved renal injury in UUO mice.

Discussion

In recent studies, a strong relationship has been reported between miRNAs and ER homeostasis, as well as UPR signaling. Gu et al. demonstrated that inhibition of miR-200b reversed high glucose-induced ER stress, UPR signaling, and apoptosis via regulation of CITED2 [35].

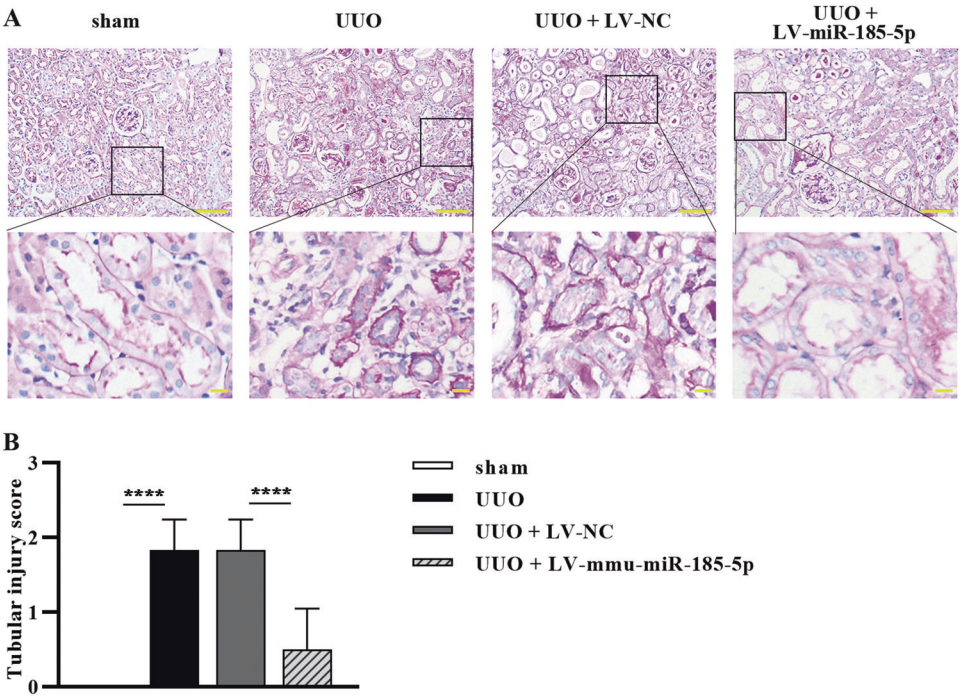

Fig. 6 Effects of miR-185-5p on renal structure in a mouse model of unilateral urethral obstruction. a Upper panel: PAS staining in the kidney of UUO mice. Scale bar, 100 μm. Lower panel: inset at a higher magnification of the image above. Scale bar, 25 μm. **b** Semiquantitative analysis of tubular injury. Data are presented as the mean ± SD ($n = 6$, one-way ANOVA with Tukey's test).

During ER stress, miR-34c-5p directly decreased the mRNA level of XBP1s, thereby regulating the proadaptive component of the UPR [36]. In the current study, we attempted to illuminate the role of miR-185-5p in renal fibrosis. We revealed that miR-185-5p suppressed ECM accumulation, alleviated ER stress, and blocked dedifferentiation in TGF-β1-induced HK2 cells, and the exertion of such roles was dependent on the downregulation of ATF6. In addition, we found that miR-185-5p ameliorated renal fibrosis using a mouse model of UUO. Our findings provided novel insights into how miR-185-5p emerged as a central regulator in renal fibrosis and the associated molecular mechanisms.

Sustained ER stress might lead to fibrosis via activation of apoptosis, induction of dedifferentiation, and inflammatory response [12, 13]. In our study, we demonstrated that miR-185-5p prevented the process of dedifferentiation through downregulation of ATF6 during renal fibrosis, which coincides with the research conducted by Xue et al. Their research showed that miR-185/DNMT1/MEG3 pathway affects dedifferentiation process in TGF-β1-induced HK2 cells [31]. Moreover, we found that miR-185-5p regulated the expression of CHOP, both in TGF-β1-induced HK2 cells and in kidneys of UUO mice. CHOP, a proapoptotic transcription factor, has been proven to regulate several proapoptotic and antiapoptotic genes, including Bcl-2 and GADD34 [37]. MiR-185-5p may regulate apoptosis during renal fibrosis depending on CHOP-mediated proapoptotic pathways. This possibility remains to be further elucidated. Regarding inflammation, it was suggested that inflammatory responses occurred in a model of diabetic nephropathy, especially TNF-α was described to cause ER stress in the kidneys of aging diabetic mice [38]. Considering the correlation of inflammation and ER stress, it would be reasonable to further investigate the possibility that miR-185-5p is involved in inflammatory responses in renal fibrosis.

In this study, we found that miR-185-5p prevented ER stress through downregulating ATF6. Moreover, miR-185-5p had an inhibitory effect on activation of the PERK/eIF2α/ATF4 branch and the IRE1/XBP1 branch. Considering that activation of ATF6 upregulated PERK signaling in colorectal cancer development [39], we hypothesized that the other two UPR branches were inactivated because of reduced ATF6 expression mediated by miR-185-5p. Therefore, we knocked down ATF6 using siRNA in TGF-β1-induced HK2 cells. Silencing of ATF6 did not affect the expression of markers in the other two UPR branches (data not shown). There may be a possibility that miR-185-5p targeted additional genes involved in the other two branches. The multiple substrates of miR-185-5p further revealed its important roles in managing ER stress, and how miR-185-5p regulated these two branches will be investigated in our future studies.

It has been validated by several studies that ATF6 can be regulated by miRNAs. For example, miR-103/107 facilitates ER stress-mediated apoptosis through targeting the Wnt3a/β-catenin/ATF6 pathway in preadipocytes [40]. MiR-199a-5p modulates UPR activation by controlling ATF6, thereby protecting cardiac myocytes during chronic hypoxia [41]. To the best of our knowledge, the current study was the first to reveal a mechanism by which ATF6

was the target gene of miR-185-5p, and downregulation of ATF6 by miR-185-5p mitigated ER stress in renal fibrosis. ATF6 consists of two isoforms, ATF6α and ATF6β. Of the two isoforms, ATF6α plays an important role in cell survival under ER stress. It has been shown that double knockouts of ATF6α and ATF6β result in embryonic lethality, while single deletion of ATF6α or ATF6β does not induce an aberrant phenotype. ATF6α-null mice showed reduced survival [42]. To identify which ATF6 isoform was required for miR-185-5p-modulated ER stress, further work needs to be performed.

In conclusion, in our study, we elucidated that miR-185-5p alleviated ER stress and epithelial dedifferentiation, and finally reduced renal fibrosis by downregulating ATF6. The miR-185-5p/ATF6 pathway was proposed as a novel regulatory mechanism for renal fibrosis, and provided a potential therapeutic strategy for renal fibrosis associated with ER stress.

Acknowledgements This study was supported by grants from the National Natural Science Foundation of China (No. 81870505), the Guide Project for Natural Science Foundation of Liaoning Province (No. 20180550610), the Joint Foundation for Natural Science, Medicine, and Health of Liaoning Province (No. 20180530088), the Support Project for Innovation Talent of Department of Education, Liaoning Province (2018), and the Fund for Scientific Research of The First Hospital of China Medical University (No. FHCMU-FSR0816).

Compliance with ethical standards

Conflict of interest The authors declare that they have no conflict of interest.

Publisher's note Springer Nature remains neutral with regard to jurisdictional claims in published maps and institutional affiliations.

References

1. Liu Y. Renal fibrosis: new insights into the pathogenesis and therapeutics. Kidney Int. 2006;69:213–7.
2. Eddy AA. Molecular basis of renal fibrosis. Pediatr Nephrol. 2000;15:290–301.
3. Chevalier RL, Forbes MS, Thornhill BA. Ureteral obstruction as a model of renal interstitial fibrosis and obstructive nephropathy. Kidney Int. 2009;75:1145–52.
4. Eddy AA, Lopez-Guisa JM, Okamura DM, Yamaguchi I. Investigating mechanisms of chronic kidney disease in mouse models. Pediatr Nephrol. 2012;27:1233–47.
5. Nogueira A, Pires MJ, Oliveira PA. Pathophysiological mechanisms of renal fibrosis: a review of animal models and therapeutic strategies. In Vivo. 2017;31:1–22.
6. Harding HP, Zeng H, Zhang Y, Jungries R, Chung P, Plesken H, et al. Diabetes mellitus and exocrine pancreatic dysfunction in perk-/- mice reveals a role for translational control in secretory cell survival. Mol Cell. 2001;7:1153–63.
7. Harding HP, Zhang Y, Bertolotti A, Zeng H, Ron D. Perk is essential for translational regulation and cell survival during the unfolded protein response. Mol Cell. 2000;5:897–904.
8. Lee AH, Iwakoshi NN, Glimcher LH. XBP-1 regulates a subset of endoplasmic reticulum resident chaperone genes in the unfolded protein response. Mol Cell Biol. 2003;23:7448–59.
9. Calfon M, Zeng H, Urano F, Till JH, Hubbard SR, Harding HP, et al. IRE1 couples endoplasmic reticulum load to secretory capacity by processing the XBP-1 mRNA. Nature. 2002;415:92–96.
10. Yoshida H, Matsui T, Yamamoto A, Okada T, Mori K. XBP1 mRNA is induced by ATF6 and spliced by IRE1 in response to ER stress to produce a highly active transcription factor. Cell. 2001;107:881–91.
11. Chen X, Shen J, Prywes R. The luminal domain of ATF6 senses endoplasmic reticulum (ER) stress and causes translocation of ATF6 from the ER to the Golgi. J Biol Chem. 2002;277:13045–52.
12. Tanjore H, Lawson WE, Blackwell TS. Endoplasmic reticulum stress as a pro-fibrotic stimulus. Biochim Biophys Acta. 2013;1832:940–7.
13. Lenna S, Trojanowska M. The role of endoplasmic reticulum stress and the unfolded protein response in fibrosis. Curr Opin Rheumatol. 2012;24:663–8.
14. Taniguchi M, Yoshida H. Endoplasmic reticulum stress in kidney function and disease. Curr Opin Nephrol Hypertens. 2015;24:345–50.
15. Ke B, Zhu N, Luo F, Xu Y, Fang X. Targeted inhibition of endoplasmic reticulum stress: new hope for renal fibrosis (Review). Mol Med Rep. 2017;16:1014–20.
16. Yeh CH, Chiang HS, Lai TY, Chien CT. Unilateral ureteral obstruction evokes renal tubular apoptosis via the enhanced oxidative stress and endoplasmic reticulum stress in the rat. Neurourol Urodyn. 2011;30:472–9.
17. Chang JW, Kim H, Baek CH, Lee RB, Yang WS, Lee SK. Up-regulation of SIRT1 reduces endoplasmic reticulum stress and renal fibrosis. Nephron. 2016;133:116–28.
18. Liu QF, Ye JM, Deng ZY, Yu LX, Sun Q, Li SS. Ameliorating effect of Klotho on endoplasmic reticulum stress and renal fibrosis induced by unilateral ureteral obstruction. Iran J Kidney Dis. 2015;9:291–7.
19. Shen J, Prywes R. Dependence of site-2 protease cleavage of ATF6 on prior site-1 protease digestion is determined by the size of the luminal domain of ATF6. J Biol Chem. 2004;279:43046–51.
20. Lee K, Tirasophon W, Shen X, Michalak M, Prywes R, Okada T, et al. IRE1-mediated unconventional mRNA splicing and S2P-mediated ATF6 cleavage merge to regulate XBP1 in signaling the unfolded protein response. Genes Dev. 2002;16:452–66.
21. Ye J, Rawson RB, Komuro R, Chen X, Dave UP, Prywes R, et al. ER stress induces cleavage of membrane-bound ATF6 by the same proteases that process SREBPs. Mol Cell. 2000;6:1355–64.
22. Baek HA, Kim DS, Park HS, Jang KY, Kang MJ, Lee DG, et al. Involvement of endoplasmic reticulum stress in myofibroblastic differentiation of lung fibroblasts. Am J Respir Cell Mol Biol. 2012;46:731–9.
23. Chiang CK, Hsu SP, Wu CT, Huang JW, Cheng HT, Chang YW, et al. Endoplasmic reticulum stress implicated in the development of renal fibrosis. Mol Med. 2011;17:1295–305.
24. Valencia-Sanchez MA, Liu J, Hannon GJ, Parker R. Control of translation and mRNA degradation by miRNAs and siRNAs. Genes Dev. 2006;20:515–24.
25. Trionfini P, Benigni A, Remuzzi G. MicroRNAs in kidney physiology and disease. Nat Rev Nephrol. 2015;11:23–33.
26. Lorenzen JM, Haller H, Thum T. MicroRNAs as mediators and therapeutic targets in chronic kidney disease. Nat Rev Nephrol. 2011;7:286–94.
27. Bracken CP, Gregory PA, Kolesnikoff N, Bert AG, Wang J, Shannon MF, et al. A double-negative feedback loop between

ZEB1-SIP1 and the microRNA-200 family regulates epithelial-mesenchymal transition. Cancer Res. 2008;68:7846–54.
28. Paterson EL, Kolesnikoff N, Gregory PA, Bert AG, Khew-Goodall Y, Goodall GJ. The microRNA-200 family regulates epithelial to mesenchymal transition. ScientificWorldJournal. 2008;8:901–4.
29. Liu M, Lang N, Chen X, Tang Q, Liu S, Huang J, et al. miR-185 targets RhoA and Cdc42 expression and inhibits the proliferation potential of human colorectal cells. Cancer Lett. 2011;301:151–60.
30. Yoon JH, Choi YJ, Choi WS, Ashktorab H, Smoot DT, Nam SW, et al. GKN1-miR-185-DNMT1 axis suppresses gastric carcinogenesis through regulation of epigenetic alteration and cell cycle. Clin Cancer Res. 2013;19:4599–610.
31. Xue R, Li Y, Li X, Ma J, An C, Ma Z. miR-185 affected the EMT, cell viability, and proliferation via DNMT1/MEG3 pathway in TGF-beta1-induced renal fibrosis. Cell Biol Int. 2019;43:1152–62.
32. Kim JO, Kwon EJ, Song DW, Lee JS, Kim DH. miR-185 inhibits endoplasmic reticulum stress-induced apoptosis by targeting Na +/H+ exchanger-1 in the heart. BMB Rep. 2016;49:208–13.
33. Nangaku M, Alpers CE, Pippin J, Shankland SJ, Kurokawa K, Adler S, et al. CD59 protects glomerular endothelial cells from immune-mediated thrombotic microangiopathy in rats. J Am Soc Nephrol. 1998;9:590–7.
34. Meng XM, Nikolic-Paterson DJ, Lan HY. TGF-beta: the master regulator of fibrosis. Nat Rev Nephrol. 2016;12:325–38.
35. Gu H, Yu J, Dong D, Zhou Q, Wang JY, Fang S, et al. High glucose-repressed CITED2 expression through miR-200b triggers the unfolded protein response and endoplasmic reticulum stress. Diabetes. 2016;65:149–63.
36. Bartoszewska S, Cabaj A, Dabrowski M, Collawn JF, Bartoszewski R. miR-34c-5p modulates X-box-binding protein 1 (XBP1) expression during the adaptive phase of the unfolded protein response. FASEB J. 2019;33:11541–54.
37. Kim R, Emi M, Tanabe K, Murakami S. Role of the unfolded protein response in cell death. Apoptosis. 2006;11:5–13.
38. Wu J, Zhang R, Torreggiani M, Ting A, Xiong H, Striker GE, et al. Induction of diabetes in aged C57B6 mice results in severe nephropathy: an association with oxidative stress, endoplasmic reticulum stress, and inflammation. Am J Pathol. 2010;176:2163–76.
39. Spaan CN, Smit WL, van Lidth de Jeude JF, Meijer BJ, Muncan V, van den Brink GR, et al. Expression of UPR effector proteins ATF6 and XBP1 reduce colorectal cancer cell proliferation and stemness by activating PERK signaling. Cell Death Dis. 2019;10:490.
40. Zhang Z, Wu S, Muhammad S, Ren Q, Sun C. miR-103/107 promote ER stress-mediated apoptosis via targeting the Wnt3a/beta-catenin/ATF6 pathway in preadipocytes. J Lipid Res. 2018;59:843–53.
41. Zhou Y, Jia WK, Jian Z, Zhao L, Liu CC, Wang Y, et al. Downregulation of microRNA199a5p protects cardiomyocytes in cyanotic congenital heart disease by attenuating endoplasmic reticulum stress. Mol Med Rep. 2017;16:2992–3000.
42. Wu J, Rutkowski DT, Dubois M, Swathirajan J, Saunders T, Wang J, et al. ATF6alpha optimizes long-term endoplasmic reticulum function to protect cells from chronic stress. Dev Cell. 2007;13:351–64.